Virion structure of iflavirus slow bee paralysis virus at 2.6Å resolution

Short title: Structure of honeybee virus

Authors:
Sergei Kalynych[1], Antonín Přidal[2], Lenka Pálková[1], Yevgen Levdansky[1], Joachim R. de Miranda[3], Pavel Plevka[1,#]

1 – Structural Virology, Central European Institute of Technology, Masaryk University, Kamenice 753/5, 62500 Brno, Czech Republic
2 - Department of Zoology, Fishery, Hydrobiology, and Apidology, Faculty of Agronomy, Mendel University in Brno, Zemědělská 1/1665, 613 00 Brno, Czech Republic
3 - Department of Ecology, Swedish University of Agricultural Sciences, Uppsala, Ulls väg 16, 75651 Uppsala, Sweden

- Corresponding author
Address: Pavel Plevka, Laboratory of Structural Virology, Central European Institute of Technology, Masaryk University, Kamenice 753/5, 62500 Brno, Czech Republic
E-mail: pavel.plevka@muni.ceitec.cz
Telephone: +420 549 49 7756

Abstract (250 words)

The western honeybee (*Apis mellifera*) is the most important commercial insect pollinator. However, bees are under pressure from habitat loss, environmental stress and pathogens, including viruses that can cause lethal epidemics. Slow bee paralysis virus (SBPV) belongs to the *Iflaviridae* family of non-enveloped single-stranded RNA viruses. Here we present the structure of the SBPV virion determined from two crystal forms to resolutions of 3.4 Å and 2.6 Å. The overall structure of the virion resembles that of picornaviruses with the three major capsid proteins VP1-3 organized into a pseudo-T3 icosahedral capsid. However, the SBPV capsid protein VP3 contains a C-terminal globular domain that has not been observed in other viruses from the order *Picornavirales*. The protruding (P)-domains form "crowns" on the virion surface around each fivefold axis in one of the crystal forms. However, the P-domains are shifted 36 Å towards the threefold axis in the other crystal form. Furthermore, the P-domain contains the ser-his-asp triad within a surface patch of eight conserved residues that constitutes a putative catalytic or receptor-binding site. The movements of the domain might be required for efficient substrate cleavage or receptor binding during virus cell entry. In addition, capsid protein VP2 contains an RGD sequence that is exposed on the virion surface, indicating that integrins might be cellular receptors of SBPV.

Importance (150 words)

Pollination by honeybees is needed to sustain agricultural productivity as well as the biodiversity of wild flora. However, honeybee populations in Europe and North America have been declining since the 1950s. Honeybee viruses from the *Iflaviridae* family are among the major causes of honeybee colony mortality. We determined the virion structure of an *Iflavirus*, slow bee paralysis virus (SBPV). SBPV exhibits unique structural features not observed in other picorna-like viruses. The SBPV capsid protein VP3 has a large C-terminal domain, five of which form highly prominent protruding "crowns" on the virion surface. However, the domains can change their positions depending on the conditions of the environment. The domain includes a putative catalytic or receptor binding site that might be important for SBPV cell entry.

Keywords: colony collapse disorder, CCD, virus, Apis mellifera, honey bee, honeybee, bumblebee, Picornavirales, Iflaviridae, Iflavirus, picornavirus, virion, structure, X-ray, crystal, capsid, protein, jellyroll, inhibitor, antiviral, domain, catalytic site

Introduction

The western honeybee *Apis mellifera* plays a vital role in agriculture by providing pollination services for numerous food crops, especially those with high nutritional and economic value (1). Honeybees are also critical for maintaining the ecological and genetic diversity of wild flowering plants (2). In addition, bumblebees and several other solitary bee species are becoming increasingly important commercial pollinators of specific crops (3). However, bees and the pollination services they provide are under increasing stress due to habitat loss, intensified agricultural management, pesticides, parasites, and pathogens including numerous viruses (3). Annual honeybee colony mortality has been increasing in North America and Europe over the last couple of decades (5) which, coupled with a long-term decline in beekeeping, has become a serious threat to the adequate provision of pollination services and food security (4-6).

Honeybees are hosts to a large number of viruses, most of which persist covertly within the honeybee population interrupted by occasional outbreaks. Such outbreaks of some of the viruses can have fatal consequences for individual workers and whole colonies (7). Colony collapse disorder (CCD), a still largely unexplained rapid loss of adult bees from colonies, has been linked to virus infections (8, 9). Much of winter honeybee colony mortality is also associated with viruses (10, 11). The viruses that have the greatest impact on honeybee populations are small icosahedral picorna-like viruses from the families *Dicistroviridae* and *Iflaviridae,* including slow bee paralysis virus (SBPV), sacbrood virus (SBV), deformed wing virus (DWV), and varroa destructor virus-1 (VDV-1) (7). SBPV was discovered in 1974 (12) and was linked to honeybee colony mortality in the United Kingdom in the 1980s (13). Despite its efficient transmission by *Varroa destructor* (14), SBPV is a rare disease of honeybees (15). However, it is common in bumblebees (16, 17), and therefore honeybees may be an incidental, secondary host.

Viruses from the order *Picornavirales* have non-enveloped icosahedral virions containing a single-stranded positive-sense RNA genome about 10,000 nucleotides long (18). Picornavirus genomes are translated into polyproteins that are co- and post-translationally cleaved by viral proteases to produce structural (capsid-forming) and non-structural proteins. The capsid proteins originating from a single polyprotein form a protomer – the basic building block of the capsid. The entire capsid consists of sixty such protomers, arranged in twelve pentamer units of five protomers each. The major capsid proteins VP1-3 are arranged in a pseudo-T3 icosahedral capsid.

The only structural information available on *Iflaviridae* family members is the 25 Å resolution cryo-electron microscopy structure of the Chinese sacbrood virus (33). The structure confirmed the pseudo-T3 icosahedral symmetry of the capsid and revealed a smooth outer surface of the virion. Iflaviruses were proposed to harbor short VP4 subunits consisting of only about twenty residues (15, 34). However, because of the low molecular weight of the peptides, the existence of VP4 subunits has not been unequivocally established (15, 34). Previous genetic and proteomic analysis of iflaviruses revealed a C-terminal extension of about 160 residues in length of one of the capsid proteins (15, 34, 35). Here we present the structure of SBPV determined from two crystal forms to resolutions of 3.4 Å and 2.6 Å. The structures

110 offer the first high-resolution snapshots of a virus from the family *Iflaviridae* and of a
111 viral pathogen of the honeybee.
112

113 **Materials and Methods:**
114
115 **Virus Propagation in Honeybee Pupae**

116 Propagations of SBPV were carried out as described in the COLOSS BeeBook
117 (36). Brood areas with *Apis mellifera* white-eyed pupae were identified by colour and
118 structural features of the cell caps. White-eyed pupae were carefully extracted from
119 the brood combs, so as not to injure the pupae. The pupae were placed on paper
120 furrows with their ventral side up. In total 544 pupae were used for the SBPV
121 propagation. Virus inoculum (1µl) was injected into pupae with a Hamilton
122 micropipette with a 30-gauge 22 mm-long needle through the intersegmental cuticle
123 between the 4th and 5th sternite. Pupae that leaked haemolymph after the injection
124 were discarded. The optimal concentration of the virus in the inoculum for virus
125 production was determined experimentally, by comparing virus yields when using
126 different virus concentrations in the injection inoculum. Inoculated pupae were
127 placed into Petri dishes with the paper furrows and incubated at 30°C and 75%
128 humidity for 5 days. After incubation the pupae were frozen at -20°C. For long-term
129 storage the pupae were kept at -80°C.

130 **Virus Purification**

131 Fifty to seventy experimentally infected honeybee pupae were homogenized
132 with a Dounce homogenizer in 30 mL of phosphate-buffered saline (PBS), pH 7.5
133 (Sigma-Aldrich). The non-ionic detergent NP-40 was added to a final concentration of
134 0.5%, and the homogenate was incubated for one hour at room temperature. The
135 extract was centrifuged at 8,000g for 30 minutes. The pellet was discarded and the
136 supernatant was centrifuged at 150,000g for 3 hours in a Ti50.2 fixed-angle rotor
137 (Beckman-Coulter™). The resulting pellet was resuspended in PBS to a final volume
138 of 5 mL. $MgCl_2$ was added to a final concentration of 5 mM as well as 20 µg/mL
139 DNAse I, and 20 µg/mL RNAse. The solution was incubated at room temperature for
140 30 minutes and centrifuged at 4,000g for 15 minutes. The resulting supernatant was
141 loaded onto a CsCl (0.6 g/mL) solution prepared in PBS. The ultracentrifugation
142 proceeded for 16 hours to establish the CsCl gradient. Virus bands were collected by
143 gentle piercing of the ultracentrifuge tubes with an 18-gauge needle. The viruses
144 were transferred to PBS by several rounds of concentration and dilution using
145 centrifuge filter units with a 100 kDa molecular weight cut-off. This procedure
146 yielded about 300 µg of virus with a purity sufficient for sparse-matrix crystallization
147 screening experiments. Sample purity with respect to contaminating honeybee
148 viruses was checked by RT-qPCR, using previously reported virus-specific assays (36).
149 In both preparations, the total sum of contaminating viruses was less than 1% of the
150 virus of interest. The nucleotide sequences of the virus preparations were
151 determined by sequencing 300 ng of RNA, purified using a Qiagen RNA purification
152 kit, by IonTorrent technology and standard protocols for library preparation and
153 sequencing. The IonTorrent reads were mapped to the SBPV GenBank reference
154 sequences EU035616 (SBPV) using Tmap v4.4.8 included in TorrentSuite 4.4.2, with
155 LifeTechnologies™ recommended parameters. Variability and consensus sequences
156 were created using mpileup from samtools v.0.1.8 and an in-house script.
157

158 **SBPV crystallization**

159 SBPV crystallization screening was conducted at 4°C and 20°C with virus
160 concentrations of 5 mg/mL and 10 mg/mL. In total 2,100 conditions were tested in a
161 96-well, sitting-drop vapor diffusion format. The initial crystals that formed in 0.1M
162 NaCitrate pH 6.5, 5% (w/v) PEG 4,000 after 7 days of incubation at 20°C were
163 spherical in shape with diameters of less than 0.03 μm. The crystallization conditions
164 were optimized by using a 96-well additive screen (Hampton Research Inc.).
165 Optimized crystals with cubic morphology grew under the starting conditions with
166 extra 0.2M NDSB-221 (non-detergent sulfobetaine) and could be reproduced in a
167 hanging-drop format by mixing 1.5 µl of 10 mg/mL purified virus solution with 0.5 µl
168 of the reservoir solution. The optimized crystals were cubic in shape and required
169 three weeks to reach their final size of about 0.1 μm. The best diffraction was
170 obtained when crystals were transferred to a reservoir solution containing 10%
171 ethylene glycol prior to flash freezing in liquid nitrogen. Out of approximately 200
172 crystals tested, two crystals diffracted X-rays to a resolution of 3.4 Å.

173 Another crystal form was discovered at 4°C in 0.1M NaAcetate, pH 4.5, 5%
174 PEG-10K and contained rectangular crystals about 0.1 mm in size. The crystals could
175 be reproduced in a hanging-drop format, with some crystals reaching 0.3 mm in
176 length. The crystals were subjected to dehydration by gradually transferring the
177 coverslip containing the hanging drop to the reservoir solution containing increasing
178 concentrations of NaAcetate pH 4.5 and of PEG-10,000 as described previously (37).
179 At 20% PEG-10,000, crystals were harvested, cryo-protected in mother liquor
180 solution containing 20% glycerol and flash-frozen in liquid nitrogen. Out of 50
181 crystals screened, two crystals diffracted X-rays to a resolution of 2.6 Å.

182

183 **SBPV structure determination and refinement**

184 Diffraction data from SBPV crystal form 1 were collected at the Swiss Light
185 Source X06SA beamline equipped with Pilatus-6M detector at the wavelength of
186 1.00003 Å at 100 K using 0.1^{o} rotation per image. The crystals were of space group
187 I23. Unit cell size and packing considerations indicated that one pentamer of capsid
188 protein protomers occupied a crystallographic asymmetric unit. There are two
189 possibilities for superimposing icosahedral 532 symmetry with the 23 symmetry of
190 the crystal, which are perpendicular to each other. The orientation of the virion was
191 determined from a plot of the fivefold rotation function, calculated with the
192 program GLRF (38). Reflections between 5.0 and 4.5 Å resolution were used for the
193 calculations. Because of the superposition of the icosahedral and crystallographic
194 symmetry, the center of the particle had to be positioned at the intersection of the
195 twofold and threefold symmetry axes of the crystal. The Triatoma virus (TrV)
196 structure (PDB code 3NAP), converted to polyalanine, was used as a molecular
197 replacement model. The model was placed into the orientation and position in the
198 unit cell as described above and used to calculate phases for reflections at up to 10 Å
199 resolution, using the program CNS (39). The model-derived phases were refined by
200 25 cycles of fivefold real-space electron density map averaging using the program
201 ave (40). The mask for electron density averaging was generated by including all
202 voxels within 5 Å of any atom of the TrV model, using the program mama from the

203 package USF (41). Phase extension was applied in order to obtain phases for higher-
204 resolution reflections. The addition of a small fraction of higher-resolution data (one
205 index at a time) was followed by three cycles of averaging. This procedure was
206 repeated until phases were obtained for all the reflections, up to a resolution of 3.4
207 Å. Inspection of the map showed that the mask used for electron density averaging
208 cut the electron density of the capsid in an area around the icosahedral fivefold axis.
209 Thus, a new mask was prepared based on a correlation map calculated by comparing
210 the electron density distributions among the five NCS-related icosahedral
211 asymmetric units. The correlation map was calculated using the program coma from
212 USF (42). A cutoff value of 0.5 was used for the inclusion of voxels into the mask. The
213 surface of the correlation mask was smoothened using the program mama (42). The
214 phase extension procedure was repeated using the new mask. The resulting map
215 was of sufficient quality to allow model building.
216 The program Buccaneer was used for automated model building, utilizing the
217 fivefold non-crystallographic symmetry (NCS) present in the crystal (43, 44). The
218 model from the automated building was about 50% complete, with assigned amino
219 acid sequences. The initial model was subjected to iterative manual rebuilding using
220 the programs Coot and O (45, 46) and coordinate and B-factor refinement using the
221 programs CNS (39) and Phenix (47). No water molecules were added due to the
222 limited resolution of the diffraction data.
223 Diffraction data from SBPV crystal form 2 crystals were collected at the
224 synchrotron Soleil Proxima-1 beamline equipped with the Pilatus-6M detector at a
225 wavelength of 0.97857 Å at 100K using 0.1° rotation per image. The crystals were of
226 space group I222. The unit cell dimensions and the virus packaging considerations
227 indicated that the crystallographic asymmetric unit consists of three pentamers of
228 capsid protein protomers. Initially, a pentamer corresponding to the entire atomic
229 model of crystal form I was used as a molecular replacement model to find the
230 orientation and translation of the three pentamers in the crystallographic assymetric
231 unit using the program Phaser (48). The initial electron density map was subjected to
232 thirty cycles of non-crystallographic symmetry averaging using the program AVE (40)
233 and employing the mask based on the model from crystal form I. The averaged map
234 lacked the electron density corresponding to the protruding domain altogether,
235 which suggested that the molecular mask did not cover the correct part of the map.
236 Therefore, a correlation map was calculated, as described for crystal form I, and the
237 mask based on the correlation map was used for averaging. This map was used for
238 the automated model building in the program buccaneer (43) from the CCP4i
239 software suite (49). The geometry of the model was adjusted manually using the
240 program Coot (46). The coordinate and B-factor refinement were carried out using
241 the program CNS (39) employing strict NCS constrains.
242 In order to improve the structure of the P-domain in crystal form I, the P-
243 domain determined from crystal form II was positioned in crystal I using the program
244 Phaser (48). The model of the icosahedral asymmetric unit with the properly
245 positioned P-domain was then used to generate a new mask for real-space electron
246 density averaging in the program mama (41). Thirty cycles of real-space electron
247 density averaging were carried out using the program AVE (40). P-domain residues
248 with no corresponding density in the averaged map were manually removed using
249 the program Coot (46). The model was subjected to coordinate and B-factor DEN-

assisted refinement using the atomic model of crystal form 2 as a reference structure using the software package CNS (39, 50).

253 **Results and Discussion:**
254
255 **Structure of SBPV virion and capsid proteins**
256 The structure of SBPV was determined from two crystal forms to resolutions
257 of 3.4 Å and 2.6 Å (Table 1). The two structures are similar, with Cα-atom RMSD of
258 0.27 Å, however, they differ in the positions of protruding (P)-domains of the VP3
259 subunits on the virion surface (Fig. 1a,b). The maximum outer diameter of the virion
260 is 388 Å. The virion is bigger than those of other picornaviruses because of the P-
261 domains. The organization of capsid proteins within the SBPV virion is similar to that
262 of other viruses from the order *Picornavirales* (Fig. 1c). The capsid is built from major
263 capsid proteins VP1-3 arranged in pseudo-T3 icosahedral symmetry (Fig. 1). The
264 major capsid proteins have jellyroll β-sandwich folds with β-strands named
265 according to the picornavirus convention B to I (51). The two antiparallel β-sheets
266 forming the β-sandwich fold contain the strands BIDG and CHEF, respectively. The
267 structures of the major capsid proteins could be built except for residues 253-266 of
268 VP1, 92-100 and 261 of VP2, and 418-430 of VP3. The electron density
269 corresponding to VP4 could not be identified in either of the two structures.
270
271 **Structure of VP3 P-domain**
272 The SBPV virion represents the first atomic structure of a virus from the
273 family *Iflaviridae*. Unlike in the previously structurally characterized viruses from the
274 order *Picornavirales*, the SBPV capsid protein VP3 contains a C-terminal extension of
275 residues 267 to 430 (15) that fold into the globular P-domain positioned on the
276 capsid surface (Fig. 1c,d). The domain consists of a central twisted antiparallel β-
277 sheet formed from strands β4, β5, and β6 surrounded by the 14-residue-long α-helix
278 α1, 3-residue-long 3.10 helix, and two shorter β-sheets containing strands β1-β2 and
279 β3-β7 (Fig. 1d). The β-strands are connected by loops that vary in length between 6
280 and 23 residues. In both of the crystal forms, the residues of the P-domain have
281 higher average B-factors (crystal 1 B = 110 $Å^2$, crystal 2 B = 57 $Å^2$) than the average B
282 factors of the rest of the capsid (crystal 1 B = 57 $Å^2$, crystal 2 B = 16 $Å^2$), indicating a
283 higher mobility of the P-domain. The P-domains in the two crystal forms are similar,
284 with an RMSD of 0.32 Å for 144 Cα atoms.
285 The P-domains are positioned in different locations on the virion surface in
286 the two crystal forms (Fig. 1, 2). It is important to note that the domains are not held
287 in position by crystal contact in either of the crystal forms. In crystal form 1, five P-
288 domains related by one icosahedral fivefold axis form a "crown" on the virion
289 surface (Fig. 1a, 3a). The crowns have a diameter of 90 Å and protrude 50 Å above
290 the capsid surface, giving the SBPV virion its characteristic shape (Fig. 1a). Residues
291 from β2- β3 as well as the N- and C-terminal loops and β2 of the P-domain interact
292 with BC, CD, and the EF loops of VP1, forming an interface with a buried surface area
293 of 850 $Å^2$ (Fig. 2a,b). P-domains within the same crown do not interact with each
294 other (Fig. 1a, 3a). In crystal form 1 the electron density map corresponding to the P-
295 domains is less well ordered than that of the rest of the SBPV virion, indicating an
296 increased mobility of the crown.
297 In crystal form 2, the P-domain is positioned approximately equal distances
298 from the icosahedral fivefold, threefold and twofold axes (Fig. 1b, 3b). Residues from

299 α1, β3, β5, β7, and loops β2-β3, β3-β4, β4-β5 of the P-domain interact with the CD
300 and GH loops of VP3, C-terminus of VP1, and GH loop of VP2, forming an interface
301 with a buried surface area of 1150 $Å^2$ (Fig. 2c,d). The density of the P-domain is
302 better resolved than in crystal form 1, indicating that the P-domain forms more
303 stable interactions with the capsid surface at the interface observed in crystal form
304 2. The transition between the two alternative positions of the P-domain on the virion
305 surface requires a 122° degree rotation of the domain around the axis which passes
306 through Lys266 (Fig. 1c). The center of mass of the P-domain in crystal form 2 is
307 shifted 36 Å towards the threefold axis relative to its position in crystal form 1 (Fig.
308 1). This movement of the domain is possible due to a 23-residue-long flexible linker
309 that connects the P-domain to the core of the VP3 subunit.

310 The crystallization conditions that produced the two crystal forms of SBPV
311 differed in terms of solution components and pH, which was 6.5 for crystal form 1
312 and 4.5 for crystal form 2 (Table 1). We speculate that the differences in localization
313 of the P-domains might be induced by the differences in the crystallization
314 conditions. Furthermore, it is possible that the two observed location of the P-
315 domain on the virion surface reflect movements of the domain required for SBPV
316 cell entry *in vivo*. Similar mobility of the protruding domain was previously reported
317 for capsid proteins of mammalian caliciviruses, where it was speculated to facilitate
318 virus-receptor interactions (52-54). The cell entry of iflaviruses has not been studied,
319 but it is likely to involve receptor-mediated endocytosis as has been described for
320 mammalian picornaviruses (29, 55). The endosomal entry involves exposure of the
321 virions to low pH that could trigger movements of the P-domain that might be
322 required for cleavage of substrate by the putative catalytic triad within the P-domain
323 as described below.
324

325 **P-domain contains putative receptor-binding or catalytic site**

326 Residues ser284, his283, and asp300 from the P-domain of VP3 are located
327 close to each other, indicating the presence of a putative catalytic triad (56) that
328 might be involved in the cleavage of an as yet unknown substrate. These residues
329 face the interior of the crown in crystal form 1, however, they constitute the apex of
330 the P-domain in crystal form 2 (Fig. 3a,b). The distances between the side chains of
331 the putative reactive site are larger than ideal for catalyzing the hydrolytic reaction
332 (Fig. 3c) (56). Nevertheless, it is possible that the optimal configuration of the active
333 site might be achieved upon binding the unknown substrate to the P-domain. This
334 type of catalytic triad has been previously identified in proteases, lipases, and
335 esterases (56-58). The residues constituting the putative active site are conserved
336 among other iflaviruses that have P-domains including DWV, VDV-1, and Kakugo
337 virus (34, 59, 60). However, the iflaviruses Sacbrood and *Perina nuda* virus lack P-
338 domains altogether (61, 62). Catalytic activity of the putative active site might be
339 required for the virions to escape from endosomes in a manner analogous to the
340 lipase activity present in the N-terminal domain of capsid proteins of parvoviruses
341 (63). There are five additional conserved residues located in the vicinity of the
342 putative active site in strand β1 and loops connecting strands, β1-β2 and β1-β3 (Fig.
343 3c). This is in contrast to the overall 12% sequence identity of the P-domains. The
344 conservation of the residues reinforces the possibility that they may constitute a
345 receptor or substrate-binding site. Furthermore, a similar conserved patch of

346 residues in P-domains of noroviruses was shown to bind glycans (64, 65). Additional
347 experiments are required to identify the putative receptor of SBPV and to determine
348 whether the catalytic triad cleaves it.
349 DALI server was used to identify structures similar to the P-domain (Table 2)
350 (66). Most of the top hits were domains of virus capsid proteins that are exposed on
351 the virion surface, and therefore might be involved in receptor binding or cell entry.
352 A common feature of these domains is a core formed of β-strands that is in some
353 cases complemented by one or more short α-helices located at the periphery of the
354 domain (Fig. 4). Furthermore, the P-domains were also found in plant picorna-like
355 viruses from the family *Tombusviridae* (67). In these species, however, the
356 protrusions exhibit a β-jellyroll fold. Even though the surface domains could be
357 identified in the DALI search, the structures of the domains are quite different and
358 cannot be meaningfully superimposed. The surface domains were identified in
359 viruses from the families *Tombusviridae, Nodaviridae*, *Hepeviridae*, and *Astroviridae*
360 (67-70). All these viruses have positive-sense ssRNA genomes and similar overall
361 virion architectures. It is therefore possible that a common ancestor of these viruses
362 contained the P-domain. However, the P-domains were retained in the evolution of
363 only some of the viruses.

364 **Putative SBPV integrin receptor binding site**

365 Currently there is no information about the cell entry of honeybee viruses,
366 and the putative receptors remain to be identified. However, the VP2 subunit of
367 SBPV contains the integrin-recognition motif arg-gly-asp (RGD) in the GH loop (Fig.
368 1c). The GH loop is exposed on the virion surface in crystal form 1 but is partly
369 covered by the P-domain in crystal form 2 (Fig. 2a,b). Integrins serve as cell entry
370 receptors for numerous viruses, including human picornaviruses such as the foot and
371 mouth disease virus (FMDV) and several parechoviruses (71-73). The RGD motif
372 within the FMDV virus is located in the VP2 subunit, similar to SBPV, although closer
373 to the icosahedral twofold axis (Fig. 1c). The RGD motif is not conserved across
374 different iflaviruses and may confer specific tissue tropism to SBPV. Even though
375 honeybees encode a number of integrins (74), their involvement in virus cell entry
376 has not been demonstrated so far.
377
378 **Decreased pH does not induce formation of SBPV A particle**
379 Picornaviruses enter cells through receptor-mediated endocytosis. The
380 receptor binding and low pH of endosomes were shown to trigger the formation of
381 expanded A particles and the subsequent genome release of many picornaviruses
382 (75). The A particles are characterized by a 5-10% increase in virion radius and the
383 formation of holes in the capsid (28-32). However, the SBPV virion structures
384 determined at pH 6.5 and 4.5 are nearly identical in size (Table 3). Therefore, it
385 appears that the pH 4.5 of the crystallization condition was not sufficient to induce
386 formation of the SBPV A particles. The induction of SBPV genome release might
387 require binding to a receptor, or alternatively, iflaviruses might use an entirely
388 different mechanism for genome release.
389

390 **Comparison to virion structures of dicistroviruses**

391 The most notable difference between SBPV and structurally characterized
392 dicistroviruses, besides the P-domain, is in the positioning of the N-terminal arm of
393 the VP2 protein, which contributes to the interpentamer contacts within the capsid
394 (Fig. 5a-d). In SBPV, two β-strands from the N-terminal arm of VP2 extend the β-
395 sheet CHEF of a VP3 from the neighboring pentamer (Fig. 5c). In contrast, in
396 dicistroviruses represented by TrV and cricket paralysis virus (CrPV), the N-terminal
397 arm of the VP2 subunit reaches around an icosahedral twofold axis into the
398 neighboring pentamer, approaches a threefold axis and forms two β-strands that
399 extend the β-sheet CHEF of a VP3 subunit from the same pentamer (Fig. 5d) (76, 77).
400 Thus, the VP2 N-terminal arms of SBPV and dicistroviruses mediate interactions
401 between VP2 and VP3 subunits in different relative positions within their virions.
402 However, the type of interaction, *i.e.* extension of the β-sheet CHEF of VP3, is the
403 same for both the viruses, representing domain swapping of the VP2 N-terminal
404 arms. It was speculated previously that the observation of domain swapping among
405 homologous complexes is indicative of hinge movements of structural units
406 connected by the swapped domains. The alternative placements of the N-terminal
407 arms of VP2 subunits therefore indicate that pentamers of capsid proteins could
408 move relative to each other.
409 Additional differences between SBPV and dicistroviruses can be found on the
410 capsid surface. The RGD containing the GH loop of the SBPV VP2 subunit contains 30
411 residues, while in TrV and CrPV it is only 17 residues long (Fig. 5a,b) (76, 77). The
412 SBPV loop therefore elevates higher above the surface of the virion, which might be
413 required for binding to the putative integrin receptor (Fig. 1c). On the other hand,
414 the GH loop of the VP3 subunit is longer in TrV, containing 36 residues in comparison
415 to 24 in SBPV (Fig. 5a,b) (77).
416 The maturation of capsids of viruses from the order *Picornavirales* is
417 connected to a cleavage of capsid protein VP4 from the N-terminus of a precursor
418 subunit, called VP0. In picornaviruses, VP0 cleavage generates the proteins VP4 and
419 VP2, while it was suggested that in iflaviruses the precursor cleavage produces VP4
420 and VP3 (76, 77). It has been proposed that a conserved asp-asp-phe (DDF) motif,
421 present in parts of capsid proteins that are exposed to the virion cavity, is involved in
422 the VP0 cleavage (76-78). The dicistroviruses CrPV and TrV contain the DDF
423 sequence in a loop immediately following β-strand I of VP1, while TrV has an
424 additional DDF sequence, in a loop following β-strand I of VP3 (Fig. 5f) (76, 77). SBPV
425 also has two DDF sequences. One is in VP1, residues 226-228, and the second one is
426 formed by residues 239-241 of VP3 (Fig. 5e). Therefore, the locations of the DDF
427 sequences in SBPV are similar to those in TrV (Fig. 5ef). The DDF site in VP1 subunit
428 of SBPV is located within 4 Å, of the N-terminus of VP3 subunit from a neighboring
429 protomer suggesting that it might mediate the VP0 maturation cleavage (Fig. 5e).

430 **Absence of a hydrophobic pocket in VP1**

431 The VP1 subunits of enteroviruses and several other vertebrate
432 picornaviruses were indicated to contain a hydrophobic pocket that might bind a
433 putative lipid-like molecule called the "pocket factor" (26, 79). Pocket factor
434 mimetics that bind into the VP1 pocket with high affinity were shown to inhibit the
435 infection of some picornaviruses (80-83). However, such a hydrophobic pocket is not

436 formed within the VP1 subunits of SBPV. This suggests that capsid binding inhibitors
437 may not be effective as antivirals against honeybee viruses. However, compounds
438 targeting the putative his-ser-asp catalytic or receptor binding site in the P-domain
439 may prevent the infection of iflaviruses containing P-domains.
440

441 **Data deposition**

442 The atomic coordinates of the SBPV virion in crystal forms 1 and 2, together with the
443 structure factors and phases obtained by phase extension, were deposited into the
444 Protein Data Bank under the codes 5J96 and 5J98, respectively. The consensus
445 nucleotide sequence of SBPV is deposited in GenBank under the accession number
446 EU035616.
447
448 **Acknowledgement**
449
450 We wish to thank Jiří Svoboda for technical assistance with pupae preparation. We
451 wish to thank the beamline scientists at SLS and Soleil synchrotrons for their
452 outstanding technical assistance with crystal screening and data collection. We wish
453 to thank Christian Tellgren-Roth from LifeSciLabs at Uppsala University, Sweden for
454 assembling virus genome sequences and Emilia Semberg at SLU for technical
455 assistance. We wish to thank Dr. Jana Moravcová for her help with the preparation
456 of the manuscript for submission. We wish to thank Dr. Charles Sabin for his help
457 with preparation of the figure depicting genome of SBPV. This research was carried
458 out under the project CEITEC 2020 (LQ1601) with financial support from the Ministry
459 of Education, Youth and Sports of the Czech Republic under National Sustainability
460 Program II. The research leading to these results received funding from the
461 European Research Council under the European Union's Seventh Framework
462 Program (FP/2007-2013) / ERC Grant Agreement n. 355855' and from EMBO
463 installation grant #3041 to Pavel Plevka.
464

465 **References:**

466 1. **Allsopp MH, de Lange WJ, Veldtman R.** 2008. Valuing insect pollination
467 services with cost of replacement. PLoS One **3:**e3128.
468 2. **Biesmeijer JC, Roberts SP, Reemer M, Ohlemuller R, Edwards M,**
469 **Peeters T, Schaffers AP, Potts SG, Kleukers R, Thomas CD, Settele J,**
470 **Kunin WE.** 2006. Parallel declines in pollinators and insect-pollinated
471 plants in Britain and the Netherlands. Science **313:**351-354.
472 3. **Vanengelsdorp D, Meixner MD.** 2010. A historical review of managed
473 honey bee populations in Europe and the United States and the factors
474 that may affect them. J Invertebr Pathol **103 Suppl 1:**S80-95.
475 4. **van Engelsdorp D, Hayes J, Jr., Underwood RM, Pettis J.** 2008. A survey
476 of honey bee colony losses in the U.S., fall 2007 to spring 2008. PLoS One
477 **3:**e4071.
478 5. **Dainat B, Vanengelsdorp D, Neumann P.** 2012. Colony collapse
479 disorder in Europe. Environ Microbiol Rep **4:**123-125.
480 6. **Smith KM, Loh EH, Rostal MK, Zambrana-Torrelio CM, Mendiola L,**
481 **Daszak P.** 2013. Pathogens, pests, and economics: drivers of honey bee
482 colony declines and losses. Ecohealth **10:**434-445.
483 7. **Chen YP, Siede R.** 2007. Honey bee viruses. Adv Virus Res **70:**33-80.
484 8. **Vanengelsdorp D, Evans JD, Saegerman C, Mullin C, Haubruge E,**
485 **Nguyen BK, Frazier M, Frazier J, Cox-Foster D, Chen Y, Underwood R,**
486 **Tarpy DR, Pettis JS.** 2009. Colony collapse disorder: a descriptive study.
487 PLoS One **4:**e6481.
488 9. **Williams GR, Tarpy DR, vanEngelsdorp D, Chauzat MP, Cox-Foster**
489 **DL, Delaplane KS, Neumann P, Pettis JS, Rogers RE, Shutler D.** 2010.
490 Colony Collapse Disorder in context. Bioessays **32:**845-846.
491 10. **Berthound H IA, Haueter M, Radloff S, Neumann P.** 2010. Virus
492 infections and winter losses of honey bee colonies (Apis mellifera). .
493 Journal of Apicultural Research**:**60-65.
494 11. **Genersh E. vdO, W, Kaatz H, Schroeder A, Otten C, Buchler R, Berg S,**
495 **Ritter W, Muhlen W, Gisder S, Meixner M, Leibig G, Rosenkranz P.**
496 2010. The German bee monitoring project: a long term study to
497 understand periodically high winter losses of honey bee colonies.
498 Adipologie**:**332-352.
499 12. **Bailey L, Woods RD.** 1974. Three previously undescribed viruses from
500 the honey bee. J Gen Virol **25:**175-186.
501 13. **Carreck NL BB, Wilson JK, Allen MF. .** 2005. The epodemiology of slow
502 paralysis virus in honey bee colonies infested by Varroa destructor in the
503 UK. Proceedings of XXXIXth International Apicultural Congress, Dublin,
504 Ireland**:**32-33.
505 14. **Santillan-Galicia MT, Ball, B. V., Clark, S. J., Alderson, P. G. .** 2010.
506 Transmission of deformed wing virus and slow paralysis virus to adult
507 bees (Apis mellifera L.) by Varroa destructor. Journal of Apicultural
508 Research **49:**141-148.
509 15. **de Miranda JR, Dainat B, Locke B, Cordoni G, Berthoud H, Gauthier L,**
510 **Neumann P, Budge GE, Ball BV, Stoltz DB.** 2010. Genetic
511 characterization of slow bee paralysis virus of the honeybee (Apis
512 mellifera L.). J Gen Virol **91:**2524-2530.

513 16. **Furst MA, McMahon DP, Osborne JL, Paxton RJ, Brown MJ.** 2014.
514 Disease associations between honeybees and bumblebees as a threat to
515 wild pollinators. Nature **506:**364-366.
516 17. **McMahon DP, Furst MA, Caspar J, Theodorou P, Brown MJ, Paxton RJ.**
517 2015. A sting in the spit: widespread cross-infection of multiple RNA
518 viruses across wild and managed bees. J Anim Ecol doi:10.1111/1365-
519 2656.12345.
520 18. **Le Gall O, Christian P, Fauquet CM, King AM, Knowles NJ, Nakashima**
521 **N, Stanway G, Gorbalenya AE.** 2008. Picornavirales, a proposed order of
522 positive-sense single-stranded RNA viruses with a pseudo-T = 3 virion
523 architecture. Arch Virol **153:**715-727.
524 19. **Rossmann MG.** 1989. The canyon hypothesis. Hiding the host cell
525 receptor attachment site on a viral surface from immune surveillance. J
526 Biol Chem **264:**14587-14590.
527 20. **He Y, Chipman PR, Howitt J, Bator CM, Whitt MA, Baker TS, Kuhn RJ,**
528 **Anderson CW, Freimuth P, Rossmann MG.** 2001. Interaction of
529 coxsackievirus B3 with the full length coxsackievirus-adenovirus
530 receptor. Nat Struct Biol **8:**874-878.
531 21. **Xiao C, Bator CM, Bowman VD, Rieder E, He Y, Hebert B, Bella J, Baker**
532 **TS, Wimmer E, Kuhn RJ, Rossmann MG.** 2001. Interaction of
533 coxsackievirus A21 with its cellular receptor, ICAM-1. J Virol **75:**2444-
534 2451.
535 22. **Olson NH, Kolatkar PR, Oliveira MA, Cheng RH, Greve JM, McClelland**
536 **A, Baker TS, Rossmann MG.** 1993. Structure of a human rhinovirus
537 complexed with its receptor molecule. Proc Natl Acad Sci U S A **90:**507-
538 511.
539 23. **Rossmann MG, He Y, Kuhn RJ.** 2002. Picornavirus-receptor interactions.
540 Trends Microbiol **10:**324-331.
541 24. **Filman DJ, Syed R, Chow M, Macadam AJ, Minor PD, Hogle JM.** 1989.
542 Structural factors that control conformational transitions and serotype
543 specificity in type 3 poliovirus. EMBO J **8:**1567-1579.
544 25. **Smyth M, Tate J, Hoey E, Lyons C, Martin S, Stuart D.** 1995. Implications
545 for viral uncoating from the structure of bovine enterovirus. Nat Struct
546 Biol **2:**224-231.
547 26. **Smyth M, Pettitt T, Symonds A, Martin J.** 2003. Identification of the
548 pocket factors in a picornavirus. Arch Virol **148:**1225-1233.
549 27. **Plevka P, Perera R, Yap ML, Cardosa J, Kuhn RJ, Rossmann MG.** 2013.
550 Structure of human enterovirus 71 in complex with a capsid-binding
551 inhibitor. Proc Natl Acad Sci U S A **110:**5463-5467.
552 28. **Bakker SE, Groppelli E, Pearson AR, Stockley PG, Rowlands DJ,**
553 **Ranson NA.** 2014. Limits of structural plasticity in a picornavirus capsid
554 revealed by a massively expanded equine rhinitis A virus particle. J Virol
555 **88:**6093-6099.
556 29. **Fuchs R, Blaas D.** 2012. Productive entry pathways of human
557 rhinoviruses. Adv Virol **2012:**826301.
558 30. **Garriga D, Pickl-Herk A, Luque D, Wruss J, Caston JR, Blaas D,**
559 **Verdaguer N.** 2012. Insights into minor group rhinovirus uncoating: the
560 X-ray structure of the HRV2 empty capsid. PLoS Pathog **8:**e1002473.

561 31. **Levy HC, Bostina M, Filman DJ, Hogle JM.** 2010. Catching a virus in the
562 act of RNA release: a novel poliovirus uncoating intermediate
563 characterized by cryo-electron microscopy. J Virol **84:**4426-4441.
564 32. **Bostina M, Levy H, Filman DJ, Hogle JM.** 2011. Poliovirus RNA is
565 released from the capsid near a twofold symmetry axis. J Virol **85:**776-
566 783.
567 33. **Zhang J, Feng J, Liang Y, Chen D, Zhou ZH, Zhang Q, Lu X.** 2001. Three-
568 dimensional structure of the Chinese Sacbrood bee virus. Sci China C Life
569 Sci **44:**443-448.
570 34. **Lanzi G, de Miranda JR, Boniotti MB, Cameron CE, Lavazza A, Capucci**
571 **L, Camazine SM, Rossi C.** 2006. Molecular and biological characterization
572 of deformed wing virus of honeybees (Apis mellifera L.). J Virol **80:**4998-
573 5009.
574 35. **Geng P, Li W, Lin L, de Miranda JR, Emrich S, An L, Terenius O.** 2014.
575 Genetic characterization of a novel Iflavirus associated with vomiting
576 disease in the Chinese oak silkmoth Antheraea pernyi. PLoS One
577 **9:**e92107.
578 36. **de Miranda JR, Bailey, L., Ball, B.V., Blanchard, P., Budge, G.,**
579 **Chejanovsky, N., Chen, Y.-P., Gauthier, L., Genersch, E., De Graaf, D.,**
580 **Ribière, M., Ryabov, E., De Smet, L., van der Steen, J.J.M. .** 2013.
581 Standard methods for Apis mellifera pest and pathogen research. *In*
582 Dietemann V, Ellis, J.D., Neumann, P. (ed), The COLOSS BEEBOOK, Volume
583 II. IBRA, Treforest, UK
584 37. **Newman J.** 2006. A review of techniques for maximizing diffraction from
585 a protein crystal in stilla. Acta Crystallogr D Biol Crystallogr **62:**27-31.
586 38. **Tong L, Rossmann MG.** 1997. Rotation function calculations with GLRF
587 program. Methods Enzymol **276:**594-611.
588 39. **Brunger AT.** 2007. Version 1.2 of the Crystallography and NMR system.
589 Nat Protoc **2:**2728-2733.
590 40. **Kleywegt GJ, Read RJ.** 1997. Not your average density. Structure **5:**1557-
591 1569.
592 41. **Kleywegt GJ, Jones TA.** 1999. Software for handling macromolecular
593 envelopes. Acta Crystallogr D Biol Crystallogr **55:**941-944.
594 42. **Kleywegt GJ.** 1999. Experimental assessment of differences between
595 related protein crystal structures. Acta Crystallogr D Biol Crystallogr
596 **55:**1878-1884.
597 43. **Cowtan K.** 2006. The Buccaneer software for automated model building.
598 1. Tracing protein chains. Acta Crystallogr D Biol Crystallogr **62:**1002-
599 1011.
600 44. **Cowtan K.** 2008. Fitting molecular fragments into electron density. Acta
601 Crystallogr D Biol Crystallogr **64:**83-89.
602 45. **Jones TA, Zou JY, Cowan SW, Kjeldgaard M.** 1991. Improved methods
603 for building protein models in electron density maps and the location of
604 errors in these models. Acta Crystallogr A **47 (Pt 2):**110-119.
605 46. **Emsley P, Cowtan K.** 2004. Coot: model-building tools for molecular
606 graphics. Acta Crystallogr D Biol Crystallogr **60:**2126-2132.
607 47. **Afonine PV, Grosse-Kunstleve RW, Echols N, Headd JJ, Moriarty NW,**
608 **Mustyakimov M, Terwilliger TC, Urzhumtsev A, Zwart PH, Adams PD.**

609 2012. Towards automated crystallographic structure refinement with
610 phenix.refine. Acta Crystallogr D Biol Crystallogr **68:**352-367.
611 48. **McCoy AJ, Grosse-Kunstleve RW, Adams PD, Winn MD, Storoni LC,**
612 **Read RJ.** 2007. Phaser crystallographic software. J Appl Crystallogr
613 **40:**658-674.
614 49. **Winn MD, Ballard CC, Cowtan KD, Dodson EJ, Emsley P, Evans PR,**
615 **Keegan RM, Krissinel EB, Leslie AG, McCoy A, McNicholas SJ,**
616 **Murshudov GN, Pannu NS, Potterton EA, Powell HR, Read RJ, Vagin A,**
617 **Wilson KS.** 2011. Overview of the CCP4 suite and current developments.
618 Acta Crystallogr D Biol Crystallogr **67:**235-242.
619 50. **Brunger AT, Adams PD, Clore GM, DeLano WL, Gros P, Grosse-**
620 **Kunstleve RW, Jiang JS, Kuszewski J, Nilges M, Pannu NS, Read RJ,**
621 **Rice LM, Simonson T, Warren GL.** 1998. Crystallography & NMR system:
622 A new software suite for macromolecular structure determination. Acta
623 Crystallogr D Biol Crystallogr **54:**905-921.
624 51. **Rossmann MG, Arnold E, Erickson JW, Frankenberger EA, Griffith JP,**
625 **Hecht HJ, Johnson JE, Kamer G, Luo M, Mosser AG, et al.** 1985.
626 Structure of a human common cold virus and functional relationship to
627 other picornaviruses. Nature **317:**145-153.
628 52. **Katpally U, Voss NR, Cavazza T, Taube S, Rubin JR, Young VL, Stuckey**
629 **J, Ward VK, Virgin HWt, Wobus CE, Smith TJ.** 2010. High-resolution
630 cryo-electron microscopy structures of murine norovirus 1 and rabbit
631 hemorrhagic disease virus reveal marked flexibility in the receptor
632 binding domains. J Virol **84:**5836-5841.
633 53. **Taube S, Rubin JR, Katpally U, Smith TJ, Kendall A, Stuckey JA, Wobus**
634 **CE.** 2010. High-resolution x-ray structure and functional analysis of the
635 murine norovirus 1 capsid protein protruding domain. J Virol **84:**5695-
636 5705.
637 54. **Prasad BV, Hardy ME, Dokland T, Bella J, Rossmann MG, Estes MK.**
638 1999. X-ray crystallographic structure of the Norwalk virus capsid.
639 Science **286:**287-290.
640 55. **Bergelson JM, Coyne CB.** 2013. Picornavirus entry. Adv Exp Med Biol
641 **790:**24-41.
642 56. **Dodson G, Wlodawer A.** 1998. Catalytic triads and their relatives. Trends
643 Biochem Sci **23:**347-352.
644 57. **Canaan S, Roussel A, Verger R, Cambillau C.** 1999. Gastric lipase:
645 crystal structure and activity. Biochim Biophys Acta **1441:**197-204.
646 58. **Vaquero ME, Barriuso J, Martinez MJ, Prieto A.** 2016. Properties,
647 structure, and applications of microbial sterol esterases. Appl Microbiol
648 Biotechnol **100:**2047-2061.
649 59. **Ongus JR, Peters D, Bonmatin JM, Bengsch E, Vlak JM, van Oers MM.**
650 2004. Complete sequence of a picorna-like virus of the genus Iflavirus
651 replicating in the mite Varroa destructor. J Gen Virol **85:**3747-3755.
652 60. **Fujiyuki T, Takeuchi H, Ono M, Ohka S, Sasaki T, Nomoto A, Kubo T.**
653 2004. Novel insect picorna-like virus identified in the brains of aggressive
654 worker honeybees. J Virol **78:**1093-1100.
655 61. **Bailey L, Gibbs AJ, Woods RD.** 1964. Sacbrood Virus of the Larval Honey
656 Bee (Apis Mellifera Linnaeus). Virology **23:**425-429.

657 62. **Wu CY, Lo CF, Huang CJ, Yu HT, Wang CH.** 2002. The complete genome
658 sequence of Perina nuda picorna-like virus, an insect-infecting RNA virus
659 with a genome organization similar to that of the mammalian
660 picornaviruses. Virology **294:**312-323.
661 63. **Farr GA, Zhang LG, Tattersall P.** 2005. Parvoviral virions deploy a
662 capsid-tethered lipolytic enzyme to breach the endosomal membrane
663 during cell entry. Proc Natl Acad Sci U S A **102:**17148-17153.
664 64. **Cao S, Lou Z, Tan M, Chen Y, Liu Y, Zhang Z, Zhang XC, Jiang X, Li X,**
665 **Rao Z.** 2007. Structural basis for the recognition of blood group
666 trisaccharides by norovirus. J Virol **81:**5949-5957.
667 65. **Hansman GS, Shahzad-Ul-Hussan S, McLellan JS, Chuang GY, Georgiev**
668 **I, Shimoike T, Katayama K, Bewley CA, Kwong PD.** 2012. Structural
669 basis for norovirus inhibition and fucose mimicry by citrate. J Virol
670 **86:**284-292.
671 66. **Holm L, Rosenstrom P.** 2010. Dali server: conservation mapping in 3D.
672 Nucleic Acids Res **38:**W545-549.
673 67. **Morgunova E, Dauter Z, Fry E, Stuart DI, Stel'mashchuk V, Mikhailov**
674 **AM, Wilson KS, Vainshtein BK.** 1994. The atomic structure of Carnation
675 Mottle Virus capsid protein. FEBS Lett **338:**267-271.
676 68. **York RL, Yousefi PA, Bogdanoff W, Haile S, Tripathi S, DuBois RM.**
677 2015. Structural, Mechanistic, and Antigenic Characterization of the
678 Human Astrovirus Capsid. J Virol **90:**2254-2263.
679 69. **Chen NC, Yoshimura M, Guan HH, Wang TY, Misumi Y, Lin CC,**
680 **Chuankhayan P, Nakagawa A, Chan SI, Tsukihara T, Chen TY, Chen CJ.**
681 2015. Crystal Structures of a Piscine Betanodavirus: Mechanisms of
682 Capsid Assembly and Viral Infection. PLoS Pathog **11:**e1005203.
683 70. **Guo YR, Hryc CF, Jakana J, Jiang H, Wang D, Chiu W, Zhong W, Tao YJ.**
684 2014. Crystal structure of a nematode-infecting virus. Proc Natl Acad Sci U
685 S A **111:**12781-12786.
686 71. **Jackson T, Mould AP, Sheppard D, King AM.** 2002. Integrin alphavbeta1
687 is a receptor for foot-and-mouth disease virus. J Virol **76:**935-941.
688 72. **Boonyakiat Y, Hughes PJ, Ghazi F, Stanway G.** 2001. Arginine-glycine-
689 aspartic acid motif is critical for human parechovirus 1 entry. J Virol
690 **75:**10000-10004.
691 73. **Kalynych S, Palkova L, Plevka P.** 2015. The Structure of Human
692 Parechovirus 1 Reveals an Association of the RNA Genome with the
693 Capsid. J Virol **90:**1377-1386.
694 74. **Honeybee Genome Sequencing C.** 2006. Insights into social insects from
695 the genome of the honeybee Apis mellifera. Nature **443:**931-949.
696 75. **Groppelli E, Tuthill TJ, Rowlands DJ.** 2010. Cell entry of the aphthovirus
697 equine rhinitis A virus is dependent on endosome acidification. J Virol
698 **84:**6235-6240.
699 76. **Tate J, Liljas L, Scotti P, Christian P, Lin T, Johnson JE.** 1999. The
700 crystal structure of cricket paralysis virus: the first view of a new virus
701 family. Nat Struct Biol **6:**765-774.
702 77. **Squires G, Pous J, Agirre J, Rozas-Dennis GS, Costabel MD, Marti GA,**
703 **Navaza J, Bressanelli S, Guerin DM, Rey FA.** 2013. Structure of the
704 Triatoma virus capsid. Acta Crystallogr D Biol Crystallogr **69:**1026-1037.

705 78. **Agirre J, Aloria K, Arizmendi JM, Iloro I, Elortza F, Sanchez-Eugenia R,**
706 **Marti GA, Neumann E, Rey FA, Guerin DM.** 2011. Capsid protein
707 identification and analysis of mature Triatoma virus (TrV) virions and
708 naturally occurring empty particles. Virology **409:**91-101.
709 79. **Hadfield AT, Lee W, Zhao R, Oliveira MA, Minor I, Rueckert RR,**
710 **Rossmann MG.** 1997. The refined structure of human rhinovirus 16 at
711 2.15 A resolution: implications for the viral life cycle. Structure **5:**427-
712 441.
713 80. **Smith TJ, Kremer MJ, Luo M, Vriend G, Arnold E, Kamer G, Rossmann**
714 **MG, McKinlay MA, Diana GD, Otto MJ.** 1986. The site of attachment in
715 human rhinovirus 14 for antiviral agents that inhibit uncoating. Science
716 **233:**1286-1293.
717 81. **Hadfield AT, Diana GD, Rossmann MG.** 1999. Analysis of three
718 structurally related antiviral compounds in complex with human
719 rhinovirus 16. Proc Natl Acad Sci U S A **96:**14730-14735.
720 82. **Grant RA, Hiremath CN, Filman DJ, Syed R, Andries K, Hogle JM.** 1994.
721 Structures of poliovirus complexes with anti-viral drugs: implications for
722 viral stability and drug design. Curr Biol **4:**784-797.
723 83. **Hiremath CN, Grant RA, Filman DJ, Hogle JM.** 1995. Binding of the
724 antiviral drug WIN51711 to the sabin strain of type 3 poliovirus:
725 structural comparison with drug binding in rhinovirus 14. Acta
726 Crystallogr D Biol Crystallogr **51:**473-489.
727 84. **Kleywegt GJ, Brunger AT.** 1996. Checking your imagination: applications
728 of the free R value. Structure **4:**897-904.
729 85. **O'Flaherty S, Coffey A, Edwards R, Meaney W, Fitzgerald GF, Ross RP.**
730 2004. Genome of staphylococcal phage K: a new lineage of Myoviridae
731 infecting gram-positive bacteria with a low G+C content. J Bacteriol
732 **186:**2862-2871.
733 86. **Guu TS, Liu Z, Ye Q, Mata DA, Li K, Yin C, Zhang J, Tao YJ.** 2009.
734 Structure of the hepatitis E virus-like particle suggests mechanisms for
735 virus assembly and receptor binding. Proc Natl Acad Sci U S A **106:**12992-
736 12997.
737 87. **Chen R, Neill JD, Estes MK, Prasad BV.** 2006. X-ray structure of a native
738 calicivirus: structural insights into antigenic diversity and host specificity.
739 Proc Natl Acad Sci U S A **103:**8048-8053.
740 88. **Hopper P, Harrison SC, Sauer RT.** 1984. Structure of tomato bushy stunt
741 virus. V. Coat protein sequence determination and its structural
742 implications. J Mol Biol **177:**701-713.
743
744

Tables:

Table 1. Crystallographic Data-Collection and Refinement Statistics

	Crystal Form 1	Crystal Form 2
Crystallization conditions	NaCitrate pH 6.5, 5% (v/v) PEG-4,000, 0.2M NDSB-221	Sodium acetate pH 4.5, 5% (v/v) PEG-10,000
Space group	I23	I222
a, b, c (Å)	360.7, 360.7, 360.7	340.0, 396.8, 431.7
α, β, γ (°)	90, 90, 90	90, 90, 90
Resolution (Å)*	70.7-3.41 (3.45-3.41)	49.5-2.6 (2.64-2.60)
R_{merge}*	0.31 (1.26)	0.20 (0.98)
<I> / <σI>*	5.6 (0.4)	6.0 (0.9)
Completeness *	87.4 (43.7)	88.3 (69.3)
Redundancy	6.0	6.8
No. of reflections	92,015	780,730
R_{work} @	0.339	0.274
No. of atoms #		
Protein	7029	7369
Water	0	75
Average B-factors		
Protein	73	32
Water	N/A	30
R.m.s. deviations		
Bond lengths (Å)	1.04	1.10
Bond angles (°)	0.004	0.004
Ramachandran§		
Favored (%)	94.37	94.47
Allowed (%)	5.40	5.19
Outliers (%)	0.23	0.11
Poor rotamers	1.59	0.74
Cβ deviations (%)§	0	0
Clash score§	11.57	10.47
Molprobity score§	2.11 (100th percentile)	1.92 (98th percentile)

@ - If calculated, the R_{free} value would have been very close to the R_{work} value due to the five- and fifteenfold NCS (84). Thus, all measured reflections were used in the crystallographic refinement.

- The values are for the icosahedral asymmetric unit.

* - The values in parentheses are for the highest resolution shell.

§ - According to the criterion of Molprobity (85).

756 **Table 2.** DALI search identification of proteins similar to SBPV P-domain

Structure	PDB	DALI Z score	RMSD	Sequence identity (%)
Human astrovirus capsid protein	5ewn	4,5	3,6	9
P-domain of grouper nervous necrosis virus	4rfu	4,2	3,6	5
Orsay virus	4nww	3,3	4,5	9
Hepatitis E virus capsid protein	2zzq	3,0	3,3	13

757 [#] Fraction of amino acid from the smaller of the two compared structures that could
758 be superimposed.

759

760

761 **Table 3.** Comparison of size and volume of SBPV particles determined in crystal
762 forms 1 and 2

	Mean virion radius (Å)[#]	Virion volume ($Å^3$)[&]
crystal form 1	140	6.385×10^6
crystal form 2	139	6.386×10^6

763 [#] Determined as distance of the center of mass of the icosahedral asymmetric unit
764 from the particle center.
765 [&] Volume of virion cavity calculated based on virion structures. The space occupied
766 by the unstructured parts of the capsid proteins located on the inside of the capsid
767 was calculated based on average amino acid volumes and subtracted from the cavity
768 volume.
769

770 **Figure legends:**
771 **Fig. 1.** Structure of SBPV virion and icosahedral asymmetric unit. Surface
772 representations of SBPV virions determined in crystal form 1 (A) and crystal form 2
773 (B) show differences in the positioning of the P-domains. The surfaces of the
774 particles are rainbow-colored based on the distance from the particle center.
775 Depressions are shown in blue and peaks in red. (C) Cartoon representation of SBPV
776 icosahedral asymmetric unit. VP1 is shown in blue, VP2 in green and VP3 in red. The
777 P-domain positioned as in crystal form 1 is shown in yellow and in crystal form 2 in
778 orange. Locations of fivefold, threefold, and twofold icosahedral symmetry axes are
779 indicated by pentagon, triangle, and oval, respectively. RGD motif found in the GH
780 loop of VP2 subunit is shown as space-filling model in magenta. The position of the
781 RGD motif in FMDV is indicated with a dotted black oval. The cyan oval indicates
782 position of rotation axis relating the two P-domain positions. (D) Cartoon
783 representation of P-domain rainbow colored from N-terminus in blue to C-terminus
784 in red. Names of secondary structure elements are indicated. (E) Diagram of SBPV
785 genome organization. Capsid proteins VP1, VP2, VP3 were identified based on their
786 location in the capsid according to the picornavirus convention. Predicted molecular
787 masses of capsid proteins are specified in kDa. Location of the P-domain of VP3 is
788 indicated. VPg- viral protein genome-linked, L - leader peptide, IRES - internal
789 ribosome entry site, UTR - untranslated region, $3C^{PRO}$ - 3C protease, and RdRP - RNA-
790 dependent RNA-Polymerase.
791
792 **Fig. 2.** Interactions of P-domain with the core of the SBPV capsid. P-domain
793 footprints on the SBPV surface in crystal form 1 (A) and 2 (B). The figures show 2D
794 projections of the SBPV virion surface without the P-domains. Residues of capsid
795 proteins VP1, VP2, and VP3 are outlined in blue, green, and red, respectively.
796 Residues involved in interaction with the P-domain are shown in yellow. The P-
797 domain footprints are outlined by white lines. The border of one VP2–VP3–VP1
798 protomer is indicated by a light-blue line. Inner surfaces of P-domains in crystal form
799 1 (C) and 2 (D), viewed from inside the particle. Residues interacting with the core of
800 the capsid are shown in yellow the remaining residues in red. Positions of twofold,
801 threefold, and fivefold icosahedral symmetry axes are shown as ovals, triangles, and
802 pentagons, respectively. One icosahedral asymmetric unit is outlined by a triangle.
803
804 **Fig. 3.** P-domain contains a putative ser-his-asp active site that is part of a patch of
805 residues that are conserved among iflaviruses. The conserved residues are
806 highlighted in grey in pentamers of capsid protein protomers in the conformation
807 from crystal form 1 (A) and crystal form 2 (B). Detail of the putative active site with
808 electron density contoured at 2σ (C). Sequence alignment of residues forming the
809 conserved patch in P-domain (D). Abbreviations: HEI - heliconius erato iflavirus and
810 API - antherae pernyi iflavirus. Uniprot accession numbers of the sequences used in
811 the alignment are provided.
812
813 **Fig. 4.** Protruding domains of viruses identified in DALI search based on similarity to
814 SBPV P-domain: (A) SBPV, (B) human astrovirus outer coat protein (5EWN) (68), (C)
815 grouper nervous necrosis virus (4RFU) (69), (D) orsay virus (4NWW) (70), (E) P1
816 domain of human hepatitis E virus (3HAG) (86), and (F) P1 domain of human

817 calcivirus (2GH8) (87). Protruding domain of tomato bushy stunt virus (2TBV) (88) is
818 shown for comparison, however, it was not identified in the DALI server search. β-
819 strands are shown in light grey, helices in orange, and loops in black.
820
821 **Fig. 5.** Comparison of SBPV structure to that of dicistrovirus TrV. Cartoon
822 representations of icosahedral asymmetric units of SBPV (A) and TrV (B). VP1
823 subunits are shown in blue, VP2 in green and VP3 in red. The GH loop of VP2 is
824 highlighted in magenta, the GH loop of VP3 in cyan, and the N-terminal arms of VP2
825 in yellow. Domain swapping between SBPV (C) and TrV (D) N-terminal arms of VP2
826 subunits that mediate inter-pentamer interactions. The insets show details of
827 hydrogen bonds between β2 of VP2 and βF of VP3. Location of DDF sequences,
828 which might be involved in the cleavage of VP0 to VP4 and VP3, on the inside of the
829 capsid of SBPV (E) and TrV (F).

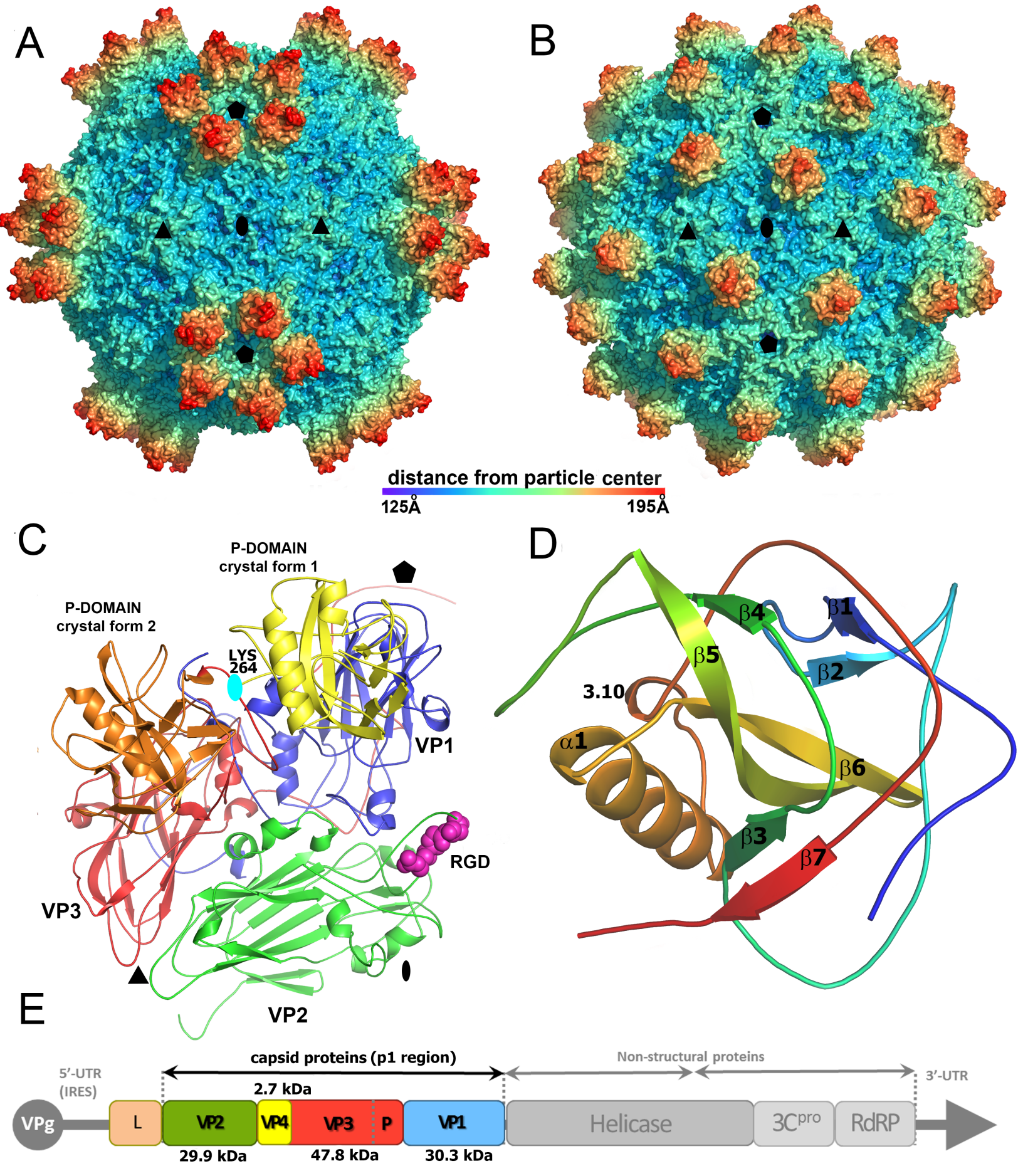
A
B
distance from particle center
125Å
195Å
C
P-DOMAIN
crystal form 1
P-DOMAIN
crystal form 2
LYS
264
VP1
RGD
VP3
VP2
D
β4
β1
β5
β2
3.10
α1
β6
β3
β7
E
5'-UTR
(IRES)
capsid proteins (p1 region)
2.7 kDa
Non-structural proteins
3'-UTR
VPg
L
VP2
VP4
VP3
P
VP1
Helicase
3Cpro
RdRP
29.9 kDa
47.8 kDa
30.3 kDa

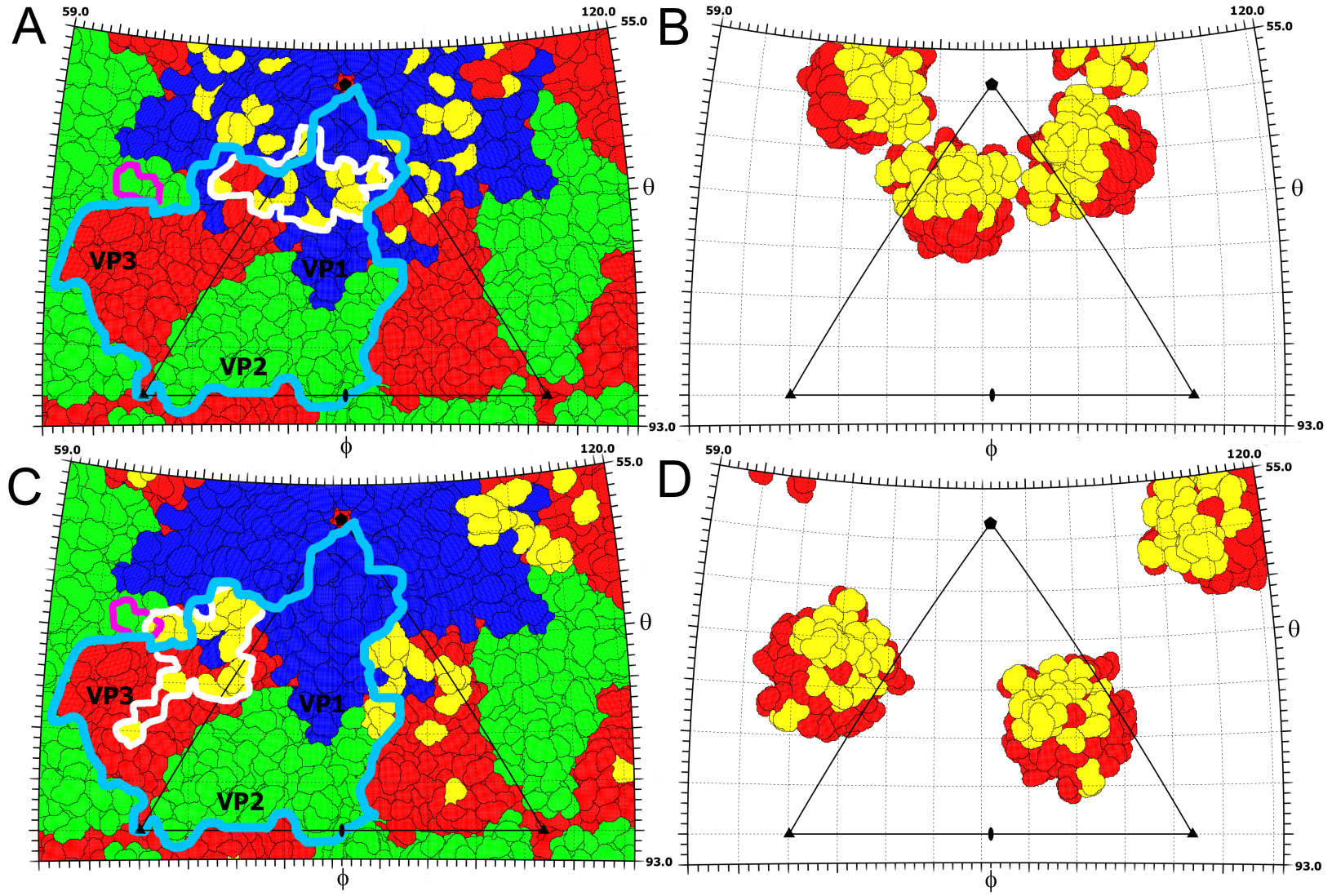
A
B
C
D
59.0
120.0
55.0
93.0
θ
ϕ
VP1
VP2
VP3

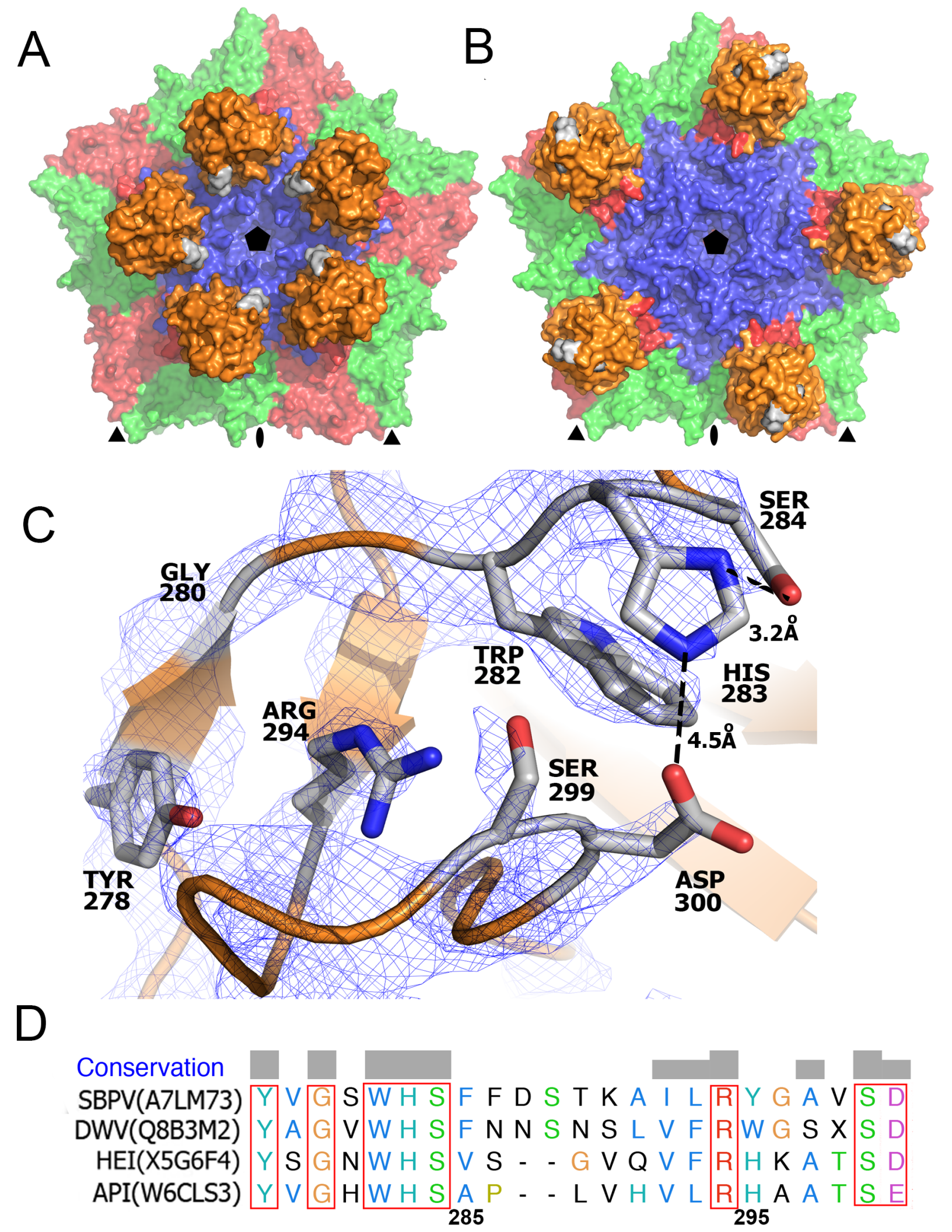
A
B
C
SER
284
GLY
280
3.2Å
TRP
282
HIS
283
ARG
294
4.5Å
SER
299
TYR
278
ASP
300
D
Conservation
SBPV(A7LM73) Y V G S W H S F F D S T K A I L R Y G A V S D
DWV(Q8B3M2) Y A G V W H S F N N S N S L V F R W G S X S D
HEI(X5G6F4) Y S G N W H S V S - - G V Q V F R H K A T S D
API(W6CLS3) Y V G H W H S A P - - L V H V L R H A A T S E
285
295

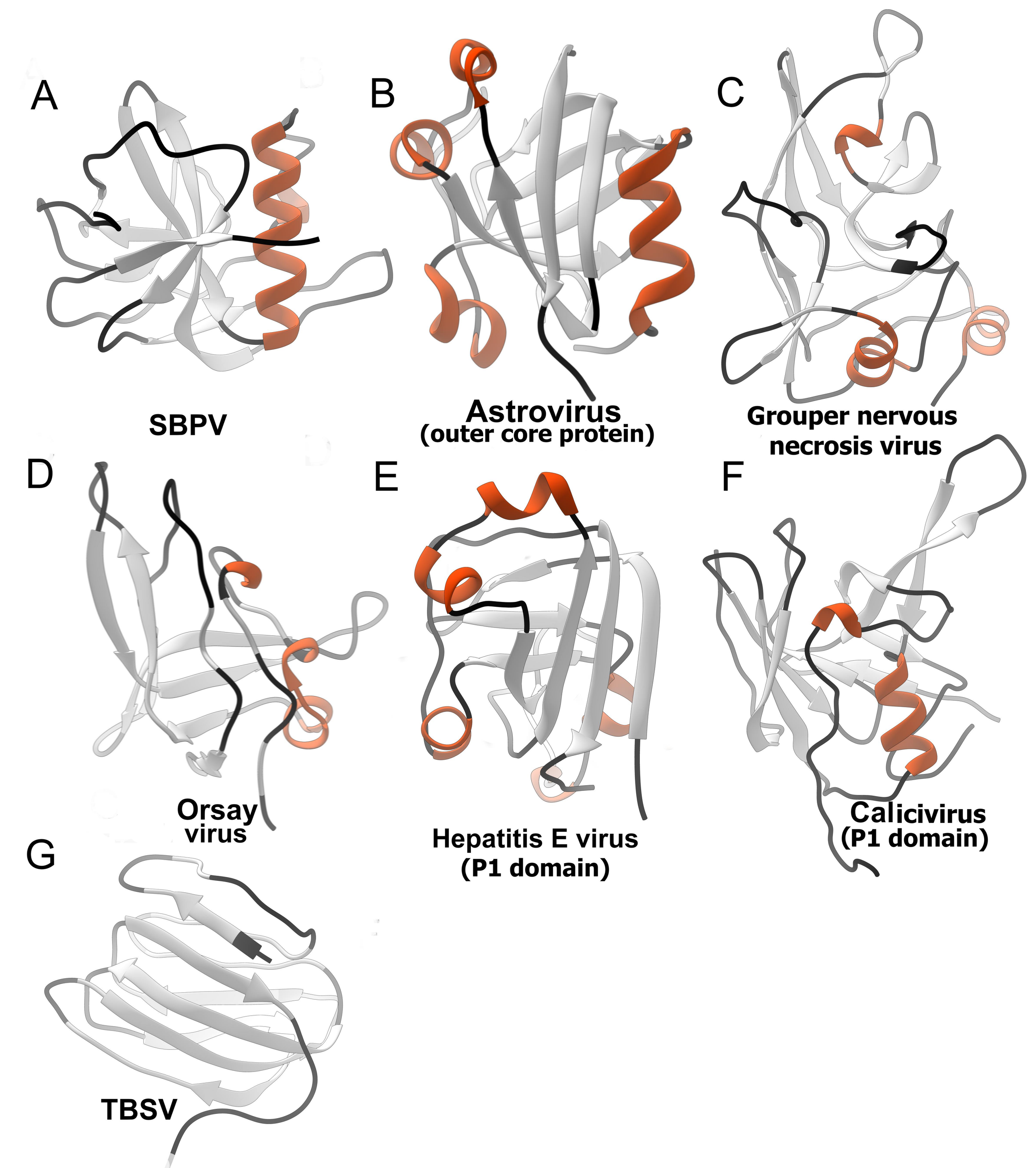
A
SBPV
B
Astrovirus
(outer core protein)
C
Grouper nervous
necrosis virus
D
Orsay
virus
E
Hepatitis E virus
(P1 domain)
F
Calicivirus
(P1 domain)
G
TBSV

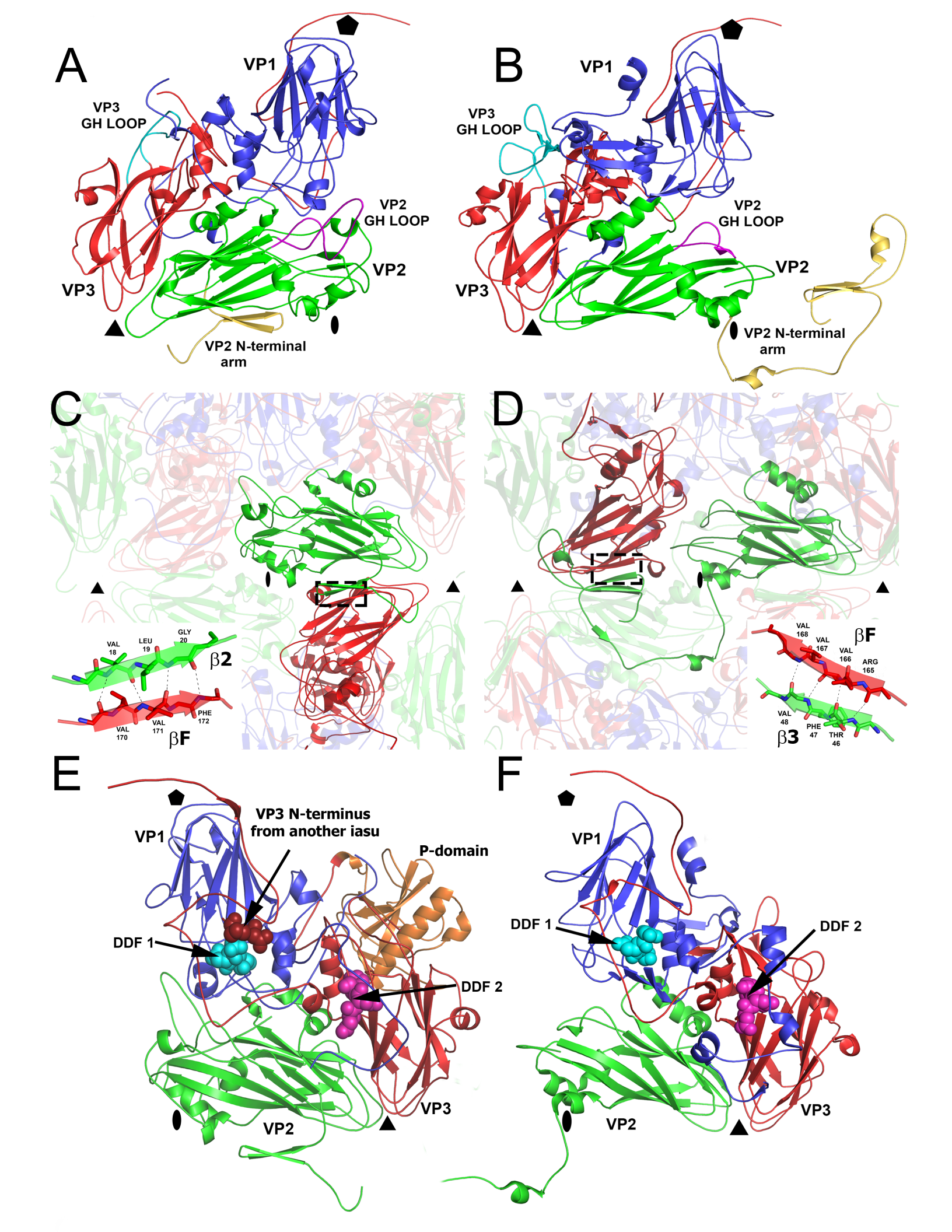
A
VP1
VP3
GH LOOP
VP2
GH LOOP
VP2
VP3
VP2 N-terminal
arm
B
VP1
VP3
GH LOOP
VP2
GH LOOP
VP2
VP3
VP2 N-terminal
arm
C
VAL
18
LEU
19
GLY
20
β2
VAL
170
VAL
171
PHE
172
βF
D
VAL
168
VAL
167
VAL
166
ARG
165
βF
VAL
48
PHE
47
THR
46
β3
E
VP3 N-terminus
from another iasu
VP1
P-domain
DDF 1
DDF 2
VP2
VP3
F
VP1
DDF 1
DDF 2
VP2
VP3